# Topochemical domain engineering to construct 2D mosaic heterostructure with internal electric field for high-performance overall water splitting

Quan Quan [a], Yuxuan Zhang [a], Fei Wang [a,c], Xiuming Bu [a], Wei Wang [a], You Meng [a], Pengshan Xie [a], Dong Chen [a], Weijun Wang [a], Dengji Li [a], Chuntai Liu [d], SenPo Yip [b], Johnny C. Ho [a,b,c,*]

[a] Department of Materials Science and Engineering, City University of Hong Kong, Kowloon 999077, Hong Kong Special Administrative Region of China
[b] Institute for Materials Chemistry and Engineering, Kyushu University, Fukuoka 816-8580, Japan
[c] State Key Laboratory of Terahertz and Millimeter Waves, City University of Hong Kong, Kowloon 999077, Hong Kong Special Administrative Region of China
[d] Key Laboratory of Advanced Materials Processing & Mold, Zhengzhou University, Ministry of Education, Zhengzhou 450002, China

## ARTICLE INFO

## ABSTRACT

Rational design of bifunctional two-dimensional (2D) heterostructures with excellent activity and durability remains a great challenge for electrocatalytic water splitting. Herein, we propose a topochemical domain engineering to realize 2D mosaic heterostructures with ultrafine phosphide nanodomains highly dispersed on the surface of Ru doped $CoMoO_4$ nanosheets (denoted as Ru-CMOP), which are vertically interconnected on the conductive skeleton assembling a 3D array structure. The as-prepared Ru-CMOP electrocatalyst exhibits excellent activity and long-term stability with the overpotentials of 114 and 286 mV at 100 mA $cm^{-2}$ for hydrogen evolution reaction (HER) and oxygen evolution reaction (OER) in 1.0 M KOH solution, respectively, outperforming most reported metal phosphide-based bifunctional heterostructures. Moreover, an assembled electrolyzer using the Ru-CMOP as anode and cathode simultaneously delivers cell voltages of 1.697 V and 1.828 V to achieve 100 mA $cm^{-2}$ and 500 mA $cm^{-2}$, respectively, with outstanding durability at 250 mA $cm^{-2}$ for 120 h. Density functional theory calculations and experimental results indicate that the strongly coupled hetero-interfaces with built-in electric field can facilitate electron transfer while multi-porous nanosheet arrays contribute to active sites exposure and mass/gas transport, thereby synergistically accelerating the reaction kinetics. Additionally, combining with a commercial silicon photovoltaic solar cell, the electrolyzer can be efficiently and robustly established, demonstrating the great potential for practical photovoltaic-electrolysis applications.

## 1. Introduction

Electrocatalytic overall water splitting to generate hydrogen and oxygen is a green and sustainable approach with zero carbon emission, which has great potential to become a crucial part of the renewable energy landscape in the future [1,2]. In this scenario, hydrogen evolution reaction (HER) and oxygen evolution reaction (OER) have been widely investigated [3], while developing efficient bifunctional electrocatalysts that yield large current densities at low overpotentials in alkaline media is challenging but paramount in terms of bringing the future water-splitting technique to reality [4,5]. The sluggish reaction kinetics of water activation are still the determinants. Toward this end,

efficient strategies are demanded to realize high-performance alkaline bifunctional electrocatalysts for industrial-scale water-splitting devices [6].

Heterostructure construction via judiciously designing hetero-interfaces has emerged as one of the most effective methods to promote intrinsic activity for surface-mediated electrochemical reactions [7–9]. Besides, a two-dimensional (2D) nanosheet structure featuring a high specific surface area is desired for the liquid-phase catalytic reaction by fully exposing accessible surfaces [10–12]. Therefore, the 2D nanosheet heterostructures have been paid much attention as they can be stronger contenders in the electrocatalytic field [13,14]. Taking 2D phosphide-based heterostructure as an example because of its excellent

activity, it can be obtained through a partial phosphorization treatment to construct an assembler with the generated phosphide onto the surface of 2D metal-based precursors [15,16]. However, the born phosphide bulks generally huddle on the surface of the 2D precursor owing to their high surface energy, which just creates another integrated surface by shielding the interfacial heterojunctions from participating in chemical reactions and limiting the reaction kinetics. Therefore, it is of significant importance to engineer the surface chemical configuration for 2D heterostructure design to transform the inert basal planes into abundant active sites [17]. In this regard, elaborately downsizing secondary phosphide building blocks onto the surface of nanosheet precursors (*e.g.*,

nanodomain modulation) provides a feasible approach for designing a 2D phosphide-based heterostructure with abundant phase boundaries and exposed active sites to boost the surface-mediated reaction kinetics.

Following the above design principle, we develop a controllable phosphorization process to in-situ produce ultrafine Ru-doped CoMoP (Ru-CMP) nanodomains uniformly dispersed on the Ru-doped $CoMoO_4$ (Ru-CMO) nanosheet arrays to construct a heterostructure (denoted as Ru-CMOP) for highly efficient overall water splitting at high current density. This method can be demonstrated as one stone with three birds: (i) the generated ultrafine Ru-CMP nanodomains with uniform distribution can activate the basal planes and create rich phase boundaries on
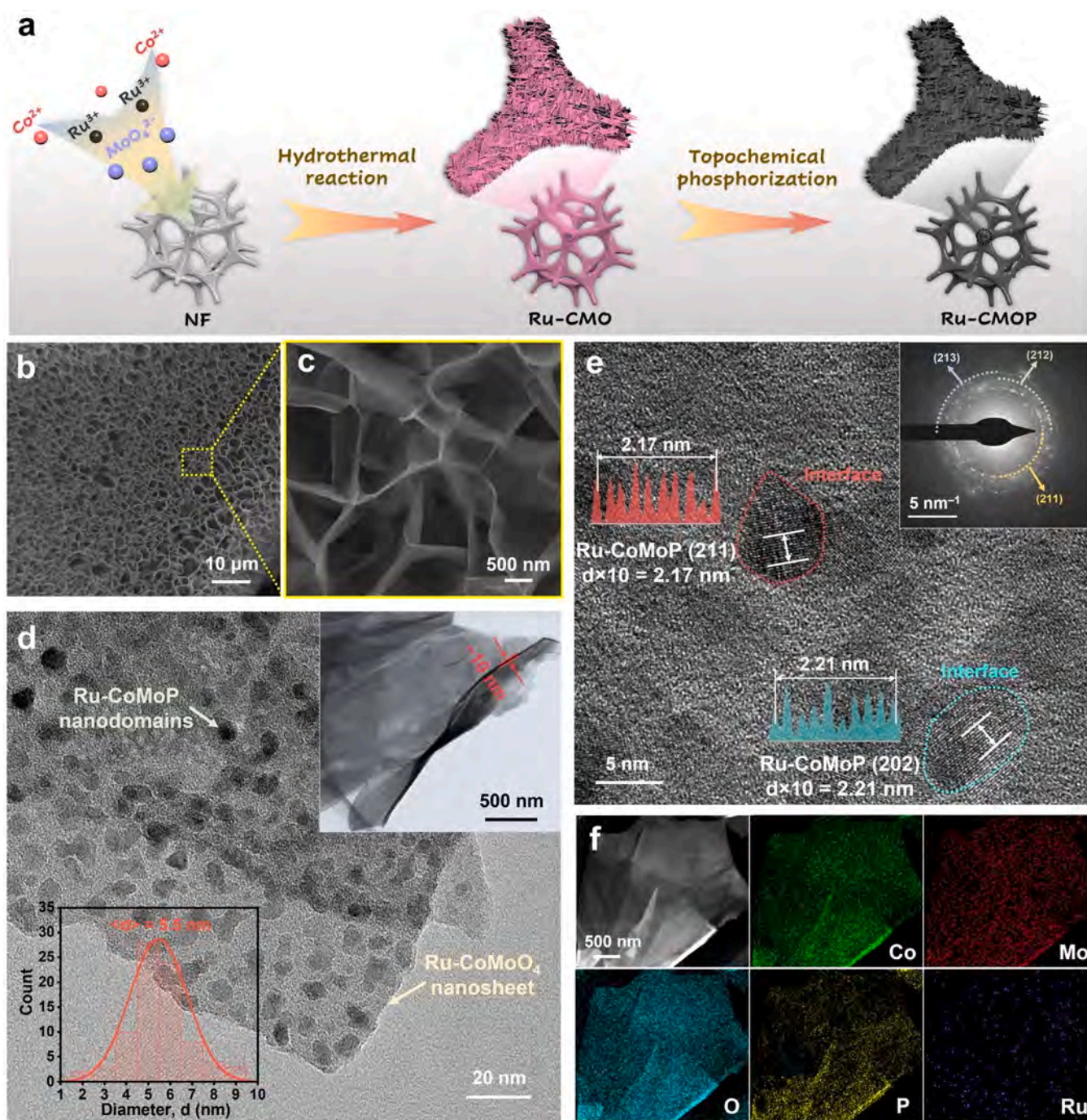


**Fig. 1.** (a) Schematic illustration for the preparation process of Ru-CMOP. (b,c) SEM, (d) TEM, and (e) HRTEM images of Ru-CMOP (insets of d: statistical calculation of diamter (lower left); TEM image of a typical Ru-CMOP nanosheet (upper right). Inset of e: SAED pattern and facet spacing details). (f) HAADF-STEM image and elemental mapping of a representative Ru-CMOP nanosheet.

Ru-CMO nanosheets to increase the number of active sites; (ii) the created heterointerfaces can form a built-in electric field and the active Ru species can also optimize the electronic structure, synergistically facilitating the electron transfer; (iii) the interconnected heterostructure nanosheet assembled as 3D multi-porous arrays can expedite the continuously produced gas bubble escape from the active sites to strengthen mechanical stability. The as-obtained Ru-CMOP exhibits an excellent HER activity with overpotentials of 114 and 183 mV at $-100$ and $-500$ mA cm$^{-2}$, respectively, and a remarkable OER activity with overpotentials of 286 and 351 mV at 100 and 500 mA cm$^{-2}$, respectively. The electrocatalyst also has long-term stability under strong reducing/oxidizing conditions. Additionally, when employed as a bifunctional catalyst for alkaline water splitting, the Ru-CMOP delivers cell voltages of 1.697 V and 1.828 V at 100 mA cm$^{-2}$ and 500 mA cm$^{-2}$, respectively, with outstanding durability at 250 mA cm$^{-2}$ for 120 h. Impressively, a solar-cell-driven overall water-splitting device is well-constructed to demonstrate its effective and robust practical operation.

## 2. Results and discussion

### 2.1. Synthesis and characterization of Ru-CMOP heterostructure

The Ru-CMOP heterostructure is synthesized through a facile two-step procedure, as illustrated in Fig. 1a. The Ru-doped CoMoO$_4$ (Ru-CMO) nanosheet arrays are firstly grown on nickel foam (NF) via a hydrothermal reaction with precisely controlling Ru doping, then subjected to a controllable phosphorization treatment through a facile gas-solid reaction [18]. As a result, the Ru doped CoMoP (Ru-CMP) nanodomains are in-situ generated on the surface of Ru-CMO nanosheets. Scanning electron microscopy (SEM) images of as-obtained Ru-CMOP exhibit a uniform 3D array structure assembled by vertically aligned 2D heterostructure nanosheets on the skeleton of NF (Fig. 1b, c and Fig. S1). Abundant spatial voids exist among the interconnected nanosheets, which are well-inherited from the structure of the Ru-CMO precursor (Fig. S2), contributing to the fast mass transfer and gas release during the electrocatalytic reaction [19]. Observed from transmission electron microscopy (TEM) images of the Ru-CMOP nanosheet, Ru-CMP nanodomains with a dark contrast can be readily distinguished, revealing that they are uniformly dispersed on the Ru-CMO phase with a large number of phase boundaries and distinct heterointerfaces (Fig. 1d and S3) [20]. The nanodomains have an average diameter of 5.5 nm and the thickness of the Ru-CMOP heterostructure is about 10 nm (insets of Fig. 1d). In Fig. 1e, the high-resolution TEM (HRTEM) image of the nanodomains exhibits the interplanar spacings of 0.217 and 0.221 nm, corresponding to the (211) and (202) planes of Ru-CoMoP crystals [21]. The corresponding selected area electron diffraction (SAED) image illustrates the polycrystalline nature of the phosphatized nanodomains [22]. In this regard, for the controllable phosphorization process, regulated PH$_3$ gas with a low dose derived from the decomposition of NaH$_2$PO$_2$ attacks the lattice of Ru-CMO precursor at the gas-solid interface. Then, the P atoms partially substitute the lattice O to generate the Ru-CMP nanodomains on the Ru-CMO sheet surface, thereby forming the 2D mosaic heterostructure with rich phase boundaries and heterointerfaces (Fig. S4) [23].

The high-angle annular dark-field scanning TEM (HAADF-STEM) and corresponding elemental mappings of the Ru-CMOP heterostructure demonstrate the coexistence and homogeneous distributions of Co, Mo, O, P elements, and slight amount of Ru dopant element across the sheet-structure in a holistic view (Fig. 1f). Additionally, as a comparative experiment, the pristine CMO counterpart without Ru doping is synthesized (Fig. S5 and S6); and then the CMOP heterostructure is obtained via an identical phosphorization process (Fig. S7 and S8). For the CMOP heterostructure, it is found that the CMP nanodomains in-situ grow on the CMO nanosheets as well but without decent dispersion, suggesting the alien Ru species are important for the nanodomains dispersion [24]. Moreover, the powder samples of Ru-CMO and Ru-CMOP are prepared

without using NF as substrates. The SEM images show that the non-uniform Ru-CMO nanosheets stack together with the lateral dimensions ranging from micrometer to nanometer scale (Fig. S9a, b). The as-obtained Ru-CMOP powders trend to agglomerate after the following phosphorization treatment, potentially decreasing the mass transfer and surface contact with electrolyte (Fig. S9c, d). In turn, these findings suggest the superiority of the self-supported sheet arrays aligned on NF skeleton with structural stability and uniformity. In a word, these results indicate the uniform generation and distribution of ultrafine Ru-CMP nanodomains on the Ru-CMO nanosheet with well-defined heterointerfaces by an intentional interface engineering, which can activate the basal planes and create rich active sites on the sheets to boost the catalytic efficiency. These 2D mosaic heterostructure nanosheets are vertically interconnected on the conductive skeleton assembling a 3D array structure with abundant porous channels.

The X-ray diffraction (XRD) result of the Ru-CMOP sample displays the pattern of the CoMoO$_4$ besides the strong peaks of metallic Ni skeleton (Fig. 2a) [25], which is identical to those of the Ru-CMO and the CMO precursors (Fig. S10). Notably, there are no peaks ascribed to the ultra-fine Ru-CMP nanodomains, suggesting their good dispersion on the 2D Ru-CMO support, in line with the results of TEM characterizations [26]. In addition, the digital photographs of samples reveal that the optical color of the electrode remarkably turns from pink to gray after the phosphorization treatment, illustrating the phase transformation (Fig. S11).

The survey XPS spectrum across a wide energy range of Ru-CMOP indicates the additional existence of P elements as compared with that of Ru-CMO, indicating the occurrence of effective phosphorization (Fig. S12a). For the depth-profiling XPS spectra of P 2p (Fig. 2b), only the P-O peak signal is detected due to the inevitable surface oxidation of metal phosphides resulting from the exposure to air. Then, the P−M (M = Co, Mo, Ru) bond at around 129.5 eV appears after the Ar ion sputtering and remains unchanged as the sputtering duration increases [27], indicating the Ru-CMP nanodomains embedded in the Ru-CMO nanosheet skeleton. Fig. 2c deconvolutes C 1 s and Ru 3d peaks in Ru-CMOP and Ru-CMO. The detected C 1 s peaks are originated from the carbon tape used in the XPS test and the contamination with environmental carbon. The binding energies of Ru 3d$_{5/2}$ and Ru 3d$_{3/2}$ peaks of the Ru-CMOP sample are centered at 281.38 and 285.78 eV, respectively [28], which is a slight shift towards lower binding energies as compared to those of Ru-CMO (Ru 3d$_{5/2}$/Ru 3d$_{3/2}$: 281.48 eV/285.88 eV). In the meanwhile, the high-resolution Co 2p spectra of the two samples can be deconvoluted into two spin-orbit doublets and two shakeup satellites (denoted as "Sat.") (Fig. 2d). For the Ru-CMOP, the first doublet at 781.24 and 783.96 eV and the second at 797.18 and 799.58 eV are attributed to Co 2p$_{3/2}$ and Co 2p$_{1/2}$, respectively [29]. It is observed that the phosphorization treatment leads to an upshift behavior of the Co 2p spectra for Ru-CMOP as compared to those of Ru-CMO. Moreover, the Mo 3d and O 1s peaks also exhibit positive shifts as compared to the Ru-CMO precursor (Fig. S12b, c). In the Mo 3d region of Ru-CMOP, two significant peaks located at 232.54 and 235.66 eV are assigned to the Mo 3d$_{5/2}$ and Mo 3d$_{3/2}$, accordingly, indicative of an oxidation state for + 6 [30]. These results signify the charge redistribution occurs after the formation of Ru-CMP nanodomains due to the strong interfacial interaction.

To further illustrate this, the differential charge density is calculated to identify the charge distribution on the Ru-CMO and Ru-CMOP (Fig. 2e). For the Ru-CMO, an accumulation charge density can be clearly visualized around the Ru doping atoms in the CMO lattice. After the addition of Ru-CMP on Ru-CMO, an obvious charge accumulation is observed at the interface between Ru-CMO and Ru-CMP, indicating the formation of a built-in electric field near the heterointerface [31], which establishes the highway of continuous electron transport between the two phases [32]. Those results demonstrate that the Ru doping and Ru-CMP assembling could induce the redistribution of the electronic structure, which results in the enhanced electron circumstances for
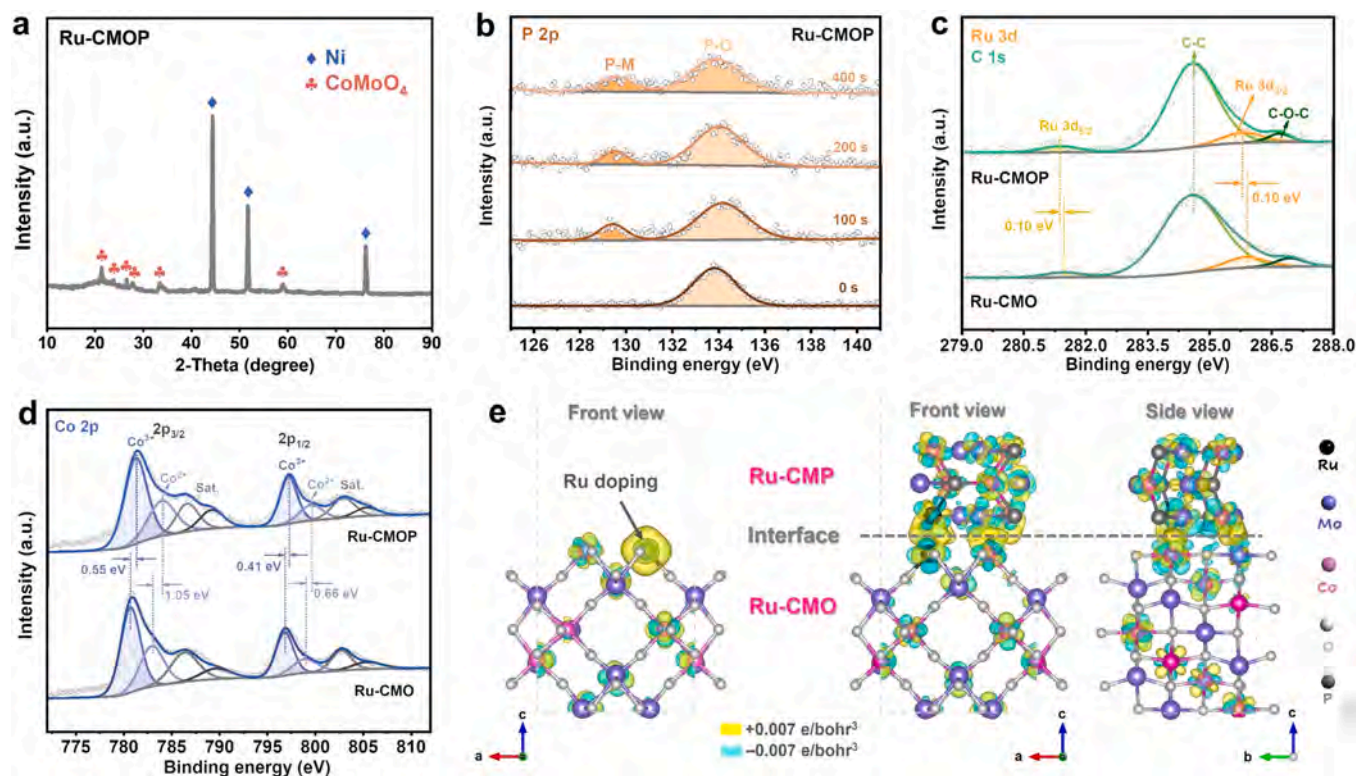
**Fig. 2.** (a) XRD pattern of Ru-CMOP. (b) Depth-profiling XPS spectra of P 2p for Ru-CMOP after Ar ion etching with different duration. (c) High-resolution XPS for Ru 3d spectra coupled with C 1 s spectra of Ru-CMOP and Ru-CMO. (d) High-resolution XPS for Co 2p spectra of Ru-CMOP and Ru-CMO. (e) Differential charge density of Ru-CMO and Ru-CMOP, where the yellow and cyan contours represent electron accumulation ($\Delta\rho = +0.007$ e × bohr$^{-3}$) and depletion ($\Delta\rho = -0.007$ e × bohr$^{-3}$), respectively.

catalyzing the electrocatalytic reaction [33].

## 2.2. HER and OER performance in alkaline media

The HER performance of the as-obtained Ru-CMOP is evaluated in an Ar-saturated 1.0 M KOH aqueous solution with a typical three-electrode system. Samples of Ru-CMO, CMOP, and CMO as counterparts and Pt/C as a benchmark are measured under identical conditions for comparison. The polarization curves of the tested catalysts for HER are presented in Fig. 3**a**. As a result, the Ru-CMOP exhibits significantly superior HER performance than the comparative samples, especially in high current density. Specifically, in comparison of CMOP (199, 232, and 280 mV), Ru-CMO (241, 275, and 332 mV), CMO (265, 315, and 426 mV), and Pt/C (193, 257, and 322 mV), Ru-CMOP delivers the current densities of 100, 200, and 500 mA cm$^{-2}$ at the low overpotentials of 114, 142 and 183 mV, respectively (Fig. 3**b**). As shown in Fig. 3**c**, the Tafel slope of Ru-CMOP exhibits the lowest value of 96 mV dec$^{-1}$ as compared with those of CMOP (108 mV dec$^{-1}$), Ru-CMO (120 mV dec$^{-1}$), CMO (197 mV dec$^{-1}$), and Pt/C (192 mV dec$^{-1}$), indicating the rapid kinetics of Ru-CMOP owing to the introduction of Ru dopant and the generation of ultrafine Ru-CMP nanodomains [34]. Besides, the Nyquist plots in Fig. S13 reveal that the Ru-CoMoP has the lowest charge transfer resistance (~ 1.4 Ω) than those of CMOP (~3.3 Ω), Ru-CMO (~21.0 Ω), and CMO (~28.8 Ω).

The double-layer capacitance ($C_{dl}$) is evaluated by cyclic voltammetry measurements, which is a widely used method to determine the electrochemically active surface area (ECSA) [35]. The highest $C_{dl}$ values of Ru-CMOP (153.5 mF cm$^{-2}$) among all catalysts (CMOP: 40.2 mF cm$^{-2}$; Ru-CMO: 1.8 mF cm$^{-2}$; Ru-CMO: 1.3 mF cm$^{-2}$) implies the maximum catalytically active sites in Ru-CMOP for HER (Fig. S14 and S15). Afterward, the stability of Ru-CMOP for HER activity is evaluated via a chronopotentiometry (CP) curve at −250 mA cm$^{-2}$ for 60 h. As

displayed in Fig. 3**f** and S16, there is no obvious potential change in this strong reducing environment for a long duration. The morphology of post-Ru-CMOP subjected to the HER stability test is well-sustained in the nanosheet-array structure (Fig. S17), suggesting the structural stability of the 3D architecture assembled from the 2D heterostructure nanosheets [36].

In the following, the OER performance of the catalysts is investigated in the Ar-saturated 1.0 M KOH solution via the three-electrode system. The commercial RuO$_2$ is applied as a benchmark sample. As shown in Fig. 3**a**, the polarization curves of the tested catalysts indicate the Ru-CMOP possesses the best catalytic activity toward the OER. In the comparison of CMOP (311, 342, and 386 mV), Ru-CMO (363, 389, and 433 mV), CMO (407, 438, and 483 mV), and RuO$_2$ (360, 389, and 442 mV), Ru-CMOP delivers the current densities of 100, 200, and 500 mA cm$^{-2}$ at the low overpotentials of 286, 317 and 351 mV, respectively (Fig. 3**d**). In Fig. 3**e**, the Tafel slope of the Ru-CMOP is calculated to be 92 mV dec$^{-1}$, which is equal to that of Ru-CMO (92 mV dec$^{-1}$) and lower than those of CMOP (103 mV dec$^{-1}$), CMO (103 mV dec$^{-1}$), and RuO$_2$ (105 mV dec$^{-1}$). This result demonstrates that the Ru doping contributes to the favorable kinetics for OER [37]. Observed from the Nyquist plots (Fig. S18), the Ru-CMOP exhibits the lowest charge transfer resistance (~1.9 Ω) as compared with CMOP (~2.9 Ω), Ru-CMO (~4.9 Ω), and CMO (~9.5 Ω). Additionally, the $C_{dl}$ value of Ru-CMOP is found to be 17.1 mF cm$^{-2}$, being larger than that of CMOP (14.2 mF cm$^{-2}$), Ru-CMO (5.4 mF cm$^{-2}$), and CMO (3.3 mF cm$^{-2}$) (Fig. S19 and S20).

Moreover, the Ru-CMOP shows decent stability at 250 mA cm$^{-2}$ for 60 h without any noticeable degradation in the alkaline media (Fig. 3**f**). The polarization curves of Ru-CMOP after the OER stability test reveal that there is a small increment of overpotential (~16 mV) at 100 mA cm$^{-2}$, implying the good stability of the catalyst for the strong and long-term OER process (Fig. S21) [27]. The SEM and TEM images of
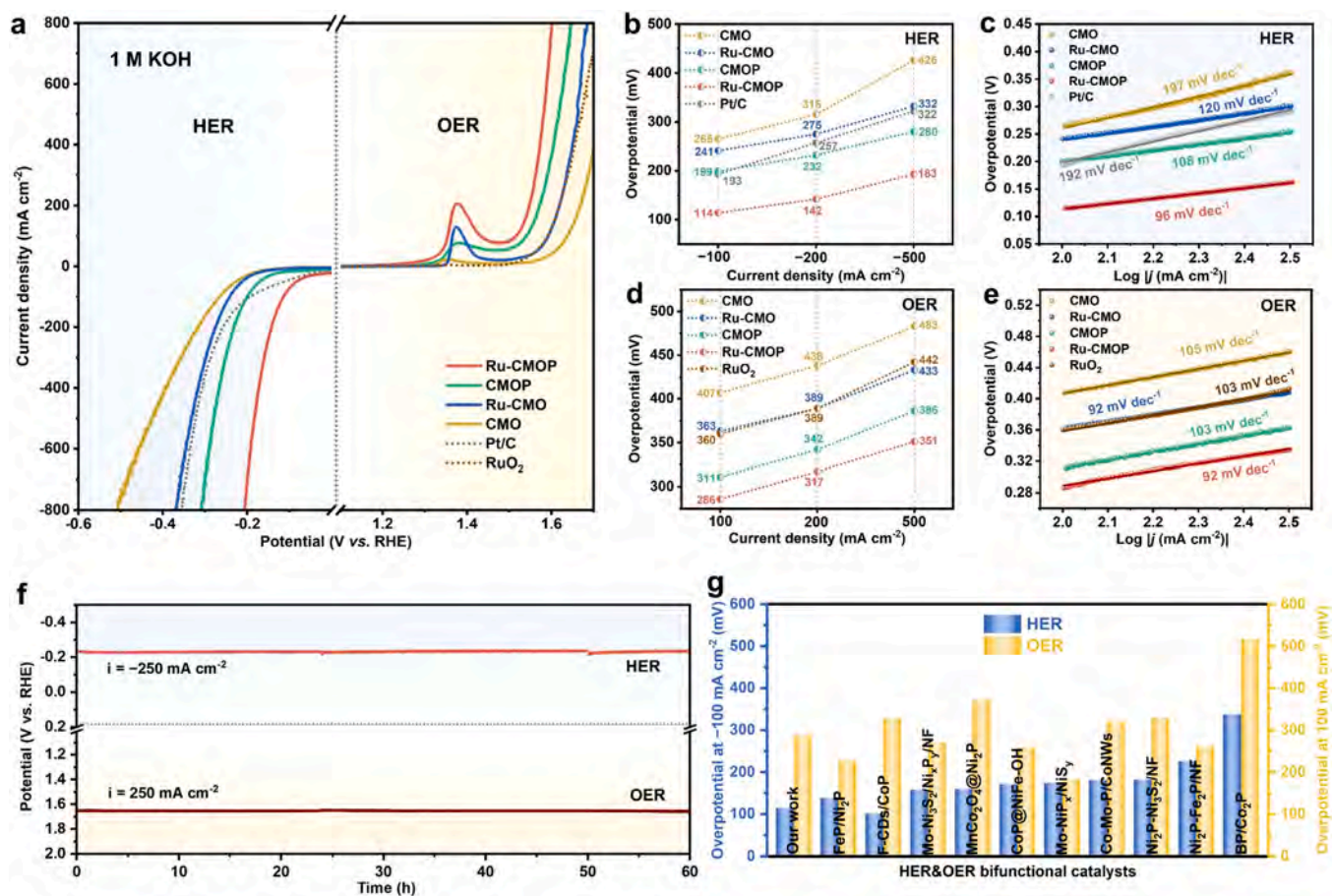
**Fig. 3.** (a) Polarization curves for HER and OER in 1 M KOH solution. Overpotentials comparison of different current densities and the corresponding Tafel plots for (b,c) HER performance and (d,e) OER performance. (f) CP curves of Ru-CMOP without iR correction at −250 mA cm$^{-2}$ and 250 mA cm$^{-2}$. (g) Comparison of overpotentials at −100/100 mA cm$^{-2}$ with the reported phosphide-based bifunctional heterostructures.

Ru-CMOP subjected to the OER stability disclose the maintained sheet-array structure with newborn particles on the sheet surface [38], which could be ascribed to the formation of cobalt oxyhydroxides as real active sites for OER (Fig. S22 and S23), consistent with the previous reports [39]. Moreover, new broad peaks for Ru-CMOP subjected to the OER stability test are emerged at around 500 and 600 cm$^{-1}$ in Raman spectra, revealing the generation of cobalt oxyhydroxides on the surface (Fig. S24) [40]. Additionally, as shown in Fig. 3g and Table S1, the excellent electrocatalytic activity of Ru-CMOP for both HER and OER in alkaline solution outperforms most of the reported phosphide-based bifunctional heterostructures, suggesting that Ru-CMOP is a promising candidate for overall water splitting.

## 2.3. Overall water splitting application

A two-electrode configuration using Ru-CMOP as both anode and cathode is built for overall water splitting in 1.0 M KOH electrolyte, which is denoted as Ru-CMOP||Ru-CMOP. Similarly, the CMOP||CMOP, Ru-CMO||Ru-CMO, and CMO||CMO two-electrode configurations are also constructed for comparison. As shown in Fig. 4a, the Ru-CMOP||Ru-CMOP exhibits the smallest cell voltage of 1.697 V to reach a current density of 100 mA cm$^{-2}$ superior to those of the CMOP||CMOP (1.809 V), Ru-CMO||Ru-CMO (1.846 V), and CMO||CMO (1.929 V). Notably, the Ru-CMOP||Ru-CMOP delivers high current densities of 200 and 500 mA cm$^{-2}$ achieved by a cell voltage of 1.748 and 1.828 V, respectively (Fig. S25). Furthermore, the durability of this Ru-CMOP|| Ru-CMOP electrolyzer is examined at a high current density of 250 mA cm$^{-2}$. As a result, the CP curve illustrates that the Ru-CMOP||

Ru-CMOP couple maintains a steady cell voltage at 250 mA cm$^{-2}$ for 120 h (Fig. 4b), manifesting the excellent robustness of Ru-CMOP for overall water splitting. Taken together, the 3D array structure is assembled by the interconnected 2D Ru-CMOP heterostructure nanosheets, where the inert surface of oxide sheets is embedded by ultrafine phosphide nanodomains as rich catalytic active sites to facilitate the efficiency of overall water splitting (Fig. 4c). Moreover, such nanosheet arrays feature abundant multi-level porosity as open channels for mass diffusion and gas release, thereby endowing a large contact area with electrolyte to further promote the electrocatalytic activity and preventing structure destruction from the bubble accumulation to strengthen the mechanical stability [41].

To further understand the electrocatalytic performance of Ru-CMOP, the total density of states (DOS) of the CMO, CMP, CMOP, and Ru-CMOP are calculated to investigate the electronic structures (Fig. 4d). As compared with single CMO and CMP, the CMOP heterostructure exhibits more states at the Fermi level. It can be deduced that new states are brought in around the Fermi level due to the strongly coupled electron orbitals near the heterointerface between CMO and CMP [42]. Hence, electrons are more probably transferred to higher unoccupied states via the enhanced transition states, contributing to a better conductivity of the CMOP hetero-system [43]. Moreover, the DOS states of Ru-CMOP near the Fermi level are higher than that of CMOP, confirming that Ru doping can further optimize the electron distribution with faster electron transfer within the heterostructure, which is consistent with the calculation results of differential charge density [44,45]. Therefore, the constructed strong heterointerfaces and the Ru doping can synergistically facilitate the electron transfer of the 2D heterostructures to
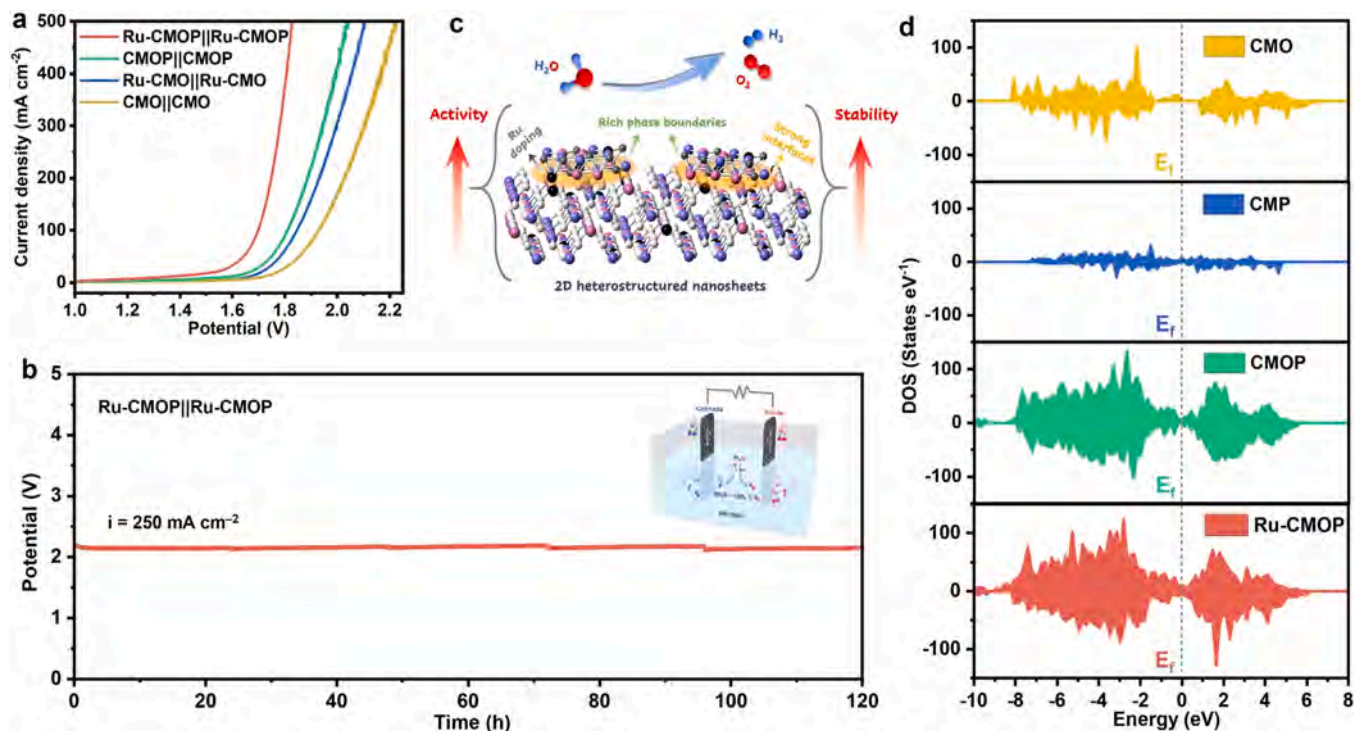
**Fig. 4.** (a) Polarization curves conducted on a two-electrode configuration for overall water splitting in 1.0 M KOH. (b) CP curve of Ru-CMOP‖Ru-CMOP couple without iR correction at 250 mA cm$^{-2}$ (inset: schematic illustration of the two-electrode setup for overall water splitting). (c) Schematic illustration of 2D heterostructure nanosheets. (d) DOS of CMO, CMP, CMOP, and Ru-CMOP.

accelerate the efficiency of electrocatalytic water splitting.

To be verified the practical utilization potential, this Ru-CMOP‖Ru-CMOP two-electrode device is integrated with a commercial silicon solar cell for solar-driven water electrolysis. The Ru-CMOP‖Ru-CMOP couple can be effectively powered by the solar panel at the potential real-time output of ~2.00 V under sunlight irradiation with enormous bubbles violently emerging from both electrodes (Fig. S26 and Movie S1). Therefore, a solar cell-driven overall water-splitting device can be efficiently and robustly achieved by the Ru-CMOP couple, demonstrating that the Ru-CMOP possesses a good potential as a bifunctional electrocatalyst for industrial applications [46].

Supplementary material related to this article can be found online at doi:10.1016/j.nanoen.2022.107566.

## 3. Conclusion

In summary, the Ru-CMOP heterostructures are prepared by a topochemical domain engineering, which is composed of the ultrafine Ru-doped CoMoP nanodomains well-dispersed on the Ru-doped CoMoO$_4$ nanosheet arrays. The Ru-CMOP exhibits excellent bifunctional HER and OER activity with long-term durability, which can be ascribed to the enormous active sites exposure, interfacial synergy effect, facilitated charge transfer, and multi-level open channels. Specifically, the Ru-CMOP shows an excellent HER activity with overpotentials of 114 and 183 mV at − 100 and − 500 mA cm$^{-2}$, respectively, and a remarkable OER activity with overpotentials of 286 and 351 mV at 100 and 500 mA cm$^{-2}$, respectively, outperforming most of the reported transition metal phosphide-based bifunctional heterostructures. Besides, the Ru-CMOP enables the alkaline overall water-splitting at cell voltages of 1.697 V and 1.828 V to achieve 100 and 500 mA cm$^{-2}$, respectively, with decent catalytic durability at 250 mA cm$^{-2}$ for 120 h. Impressively, a solar-cell-driven overall water-splitting device can be efficiently and robustly constructed to demonstrate the great potential of bifunctional Ru-CMOP for practical application.

## CRediT authorship contribution statement

**Quan Quan**: Conceptualization, Methodology, Validation, Formal analysis, Investigation, Data curation, Writing – original draft, Writing – review & editing. **Yuxuan Zhang**: Density functional theory calculation, Writing – review & editing. **Fei Wang**, **Xiuming Bu**: Investigation, Writing – review & editing. **Wei Wang**: Writing – review & editing. **You Meng**: Writing – review & editing. **Pengshan Xie**: Writing – review & editing. **Dong Chen**: Writing – review & editing. **Weijun Wang**: Writing – review & editing. **Dengji Li**: Writing – review & editing. **Chuntai Liu**: Writing – review & editing. **SenPo Yip**: Writing – review & editing. **Johnny C. Ho**: Conceptualization, Writing – original draft, Writing – review & editing, Resources, Supervision, Funding acquisition.

## Declaration of Competing Interest

The authors declare that they have no known competing financial interests or personal relationships that could have appeared to influence the work reported in this paper.

## Data Availability

Data will be made available on request.

## Acknowledgments

## Appendix A. Supporting information

Supplementary data associated with this article can be found in the

online version at doi:10.1016/j.nanoen.2022.107566.

# References

[1] Z.-Y. Yu, Y. Duan, X.-Y. Feng, X. Yu, M.-R. Gao, S.-H. Yu, Clean and affordable hydrogen fuel from alkaline water splitting: past, recent progress, and future prospects, Adv. Mater. 33 (2021) 2007100, https://doi.org/10.1002/adma.202007100.

[2] D. Zhao, K. Sun, W.C. Cheong, L. Zheng, C. Zhang, S. Liu, X. Cao, K. Wu, Y. Pan, Z. Zhuang, B. Hu, D. Wang, Q. Peng, C. Chen, Y. Li, Synergistically interactive Pyridinic-N-MoP sites: identified active centers for enhanced hydrogen evolution in alkaline solution, Angew. Chem. Int. Ed. 59 (2020) 8982–8990, https://doi.org/10.1002/anie.201908760.

[3] S. Jiao, X. Fu, S. Wang, Y. Zhao, Perfecting the electrocatalysts via imperfections: towards large-scale deployment of water electrolysis technology, Energy Environ. Sci. 14 (2021) 1722–1770, https://doi.org/10.1039/D0EE03635H.

[4] D. Yang, Z. Su, Y. Chen, K. Srinivas, J. Gao, W. Zhang, Z. Wang, H. Lin, Electronic modulation of hierarchical spongy nanosheets toward efficient and stable water electrolysis, Small 17 (2021), e2006881, https://doi.org/10.1002/smll.202006881.

[5] S.A. Chala, M.-C. Tsai, W.-N. Su, K.B. Ibrahim, B. Thirumalraj, T.-S. Chan, J.-F. Lee, H. Dai, B.-J. Hwang, Hierarchical 3D architectured Ag nanowires shelled with NiMn-layered double hydroxide as an efficient bifunctional oxygen electrocatalyst, ACS Nano 14 (2020) 1770–1782, https://doi.org/10.1021/acsnano.9b07487.

[6] P. Zhai, P. Zhang, Y. Wu, J. Gao, B. Zhang, S. Cao, Y. Zhang, Z. Li, L. Sun, J. Hou, Engineering active sites on hierarchical transition bimetal oxides/sulfides heterostructure array enabling robust overall water splitting, Nat. Commun. 11 (2020) 5462, https://doi.org/10.1038/s41467-020-19214-w.

[7] A. Kumar, V.Q. Bui, J. Lee, A.R. Jadhav, Y. Hwang, M.G. Kim, Y. Kawazoe, H. Lee, Modulating interfacial charge density of NiP₂–FeP₂ via coupling with metallic Cu for accelerating alkaline hydrogen evolution, ACS Energy Lett. 6 (2021) 354–363, https://doi.org/10.1021/acsenergylett.0c02498.

[8] M. Fang, G. Dong, R. Wei, J.C. Ho, Hierarchical nanostructures: design for sustainable water splitting, Adv. Energy Mater. 7 (2017) 1700559, https://doi.org/10.1002/aenm.201700559.

[9] S. Riyajuddin, K. Azmi, M. Pahuja, S. Kumar, T. Maruyama, C. Bera, K. Ghosh, Super-hydrophilic hierarchical Ni-foam-graphene-carbon nanotubes-Ni₂P-CuP₂ nano-architecture as efficient electrocatalyst for overall water splitting, ACS Nano 15 (2021) 5586–5599, https://doi.org/10.1021/acsnano.1c00647.

[10] Y. Gu, A. Wu, Y. Jiao, H. Zheng, X. Wang, Y. Xie, L. Wang, C. Tian, H. Fu, Two-dimensional porous molybdenum phosphide/nitride heterojunction nanosheets for pH-universal hydrogen evolution reaction, Angew. Chem. Int. Ed. 60 (2020) 6673–6681, https://doi.org/10.1002/anie.202016102.

[11] G. Guan, M.-Y. Han, Functionalized hybridization of 2D nanomaterials, Adv. Sci. 6 (2019) 1901837, https://doi.org/10.1002/advs.201901837.

[12] Q. Quan, T. Zhang, C. Lei, B. Yang, Z. Li, J. Chen, C. Yuan, L. Lei, Y. Hou, Confined carburization-engineered synthesis of ultrathin nickel oxide/nickel heterostructured nanosheets for enhanced oxygen evolution reaction, Nanoscale 11 (2019) 22261–22269, https://doi.org/10.1039/C9NR07986F.

[13] Y. Zhao, J. Zhang, Y. Xie, B. Sun, J. Jiang, W.-J. Jiang, S. Xi, H.Y. Yang, K. Yan, S. Wang, X. Guo, P. Li, Z. Han, X. Lu, H. Liu, G. Wang, Constructing atomic heterometallic sites in ultrathin nickel-incorporated cobalt phosphide nanosheets via a boron-assisted strategy for highly efficient water splitting, Nano Lett. 21 (2021) 823–832, https://doi.org/10.1021/acs.nanolett.0c04569.

[14] I.K. Mishra, H. Zhou, J. Sun, F. Qin, K. Dahal, J. Bao, S. Chen, Z. Ren, Hierarchical CoP/Ni₅P₄/CoP microsheet arrays as a robust pH-universal electrocatalyst for efficient hydrogen generation, Energy Environ. Sci. 11 (2018) 2246–2252, https://doi.org/10.1039/C8EE01270A.

[15] S.-H. Li, M.-Y. Qi, Z.-R. Tang, Y.-J. Xu, Nanostructured metal phosphides: from controllable synthesis to sustainable catalysis, Chem. Soc. Rev. 50 (2021) 7539–7586, https://doi.org/10.1039/D1CS00323B.

[16] Z.-Z. Luo, Y. Zhang, C. Zhang, H.T. Tan, Z. Li, A. Abutaha, X.-L. Wu, Q. Xiong, K. A. Khor, K. Hippalgaonkar, J. Xu, H.H. Hng, Q. Yan, Multifunctional 0D–2D Ni₂P nanocrystals–black phosphorus heterostructure, Adv. Energy Mater. 7 (2016) 1601285, https://doi.org/10.1002/aenm.201601285.

[17] Z. Kou, T. Wang, Q. Gu, M. Xiong, L. Zheng, X. Li, Z. Pan, H. Chen, F. Verpoort, A. K. Cheetham, S. Mu, J. Wang, Rational design of holey 2D nonlayered transition metal carbide/nitride heterostructure nanosheets for highly efficient water oxidation, Adv. Energy Mater. 9 (2019) 1803768, https://doi.org/10.1002/aenm.201803768.

[18] S.-H. Li, N. Zhang, X. Xie, R. Luque, Y.-J. Xu, Stress-transfer-induced in situ formation of ultrathin nickel phosphide nanosheets for efficient hydrogen evolution, Angew. Chem. Int. Ed. 57 (2018) 13082–13085, https://doi.org/10.1002/anie.201806221.

[19] L. Yu, L. Wu, S. Song, B. McElhenny, F. Zhang, S. Chen, Z. Ren, Hydrogen generation from seawater electrolysis over a sandwich-like NiCoN=NixP=NiCoN microsheet array catalyst, ACS Energy Lett. 5 (2020) 2681–2689, https://doi.org/10.1021/acsenergylett.0c01244.

[20] Q. Gong, Y. Wang, Q. Hu, J. Zhou, R. Feng, P.N. Duchesne, P. Zhang, F. Chen, N. Han, Y. Li, C. Jin, Y. Li, S.-T. Lee, Ultrasmall and phase-pure W₂C nanoparticles for efficient electrocatalytic and photoelectrochemical hydrogen evolution, Nat. Commun. 7 (2016) 13216, https://doi.org/10.1038/ncomms13216.

[21] Y.-Y. Ma, C.-X. Wu, X.-J. Feng, H.-Q. Tan, L.-K. Yan, Y. Liu, Z.-H. Kang, E.-B. Wang, Y.-G. Li, Highly efficient hydrogen evolution from seawater by a low-cost and

[22] Q. Quan, Z. Lai, Y. Bao, X. Bu, Y. Meng, W. Wang, T. Takahashi, T. Hosomi, K. Nagashima, T. Yanagida, C. Liu, J. Lu, J.C. Ho, Self-anti-stacking 2D metal phosphide loop-sheet heterostructures by edge-topological regulation for highly efficient water oxidation, Small 17 (2021) 2006860, https://doi.org/10.1002/smll.202006860.

[23] X. Luo, P. Ji, P. Wang, R. Cheng, D. Chen, C. Lin, J. Zhang, J. He, Z. Shi, N. Li, S. Xiao, S. Mu, Interface engineering of hierarchical branched Mo-Doped Ni₃S₂/NixPy hollow heterostructure nanorods for efficient overall water splitting, Adv. Energy Mater. 10 (2020) 1903891, https://doi.org/10.1002/aenm.201903891.

[24] V.H. Hoa, D.T. Tran, S. Prabhakaran, D.H. Kim, N. Hameed, H. Wang, N.H. Kim, J. H. Lee, Ruthenium single atoms implanted continuous MoS₂-Mo₂C heterostructure for high-performance and stable water splitting, Nano Energy 88 (2021), 106277, https://doi.org/10.1016/j.nanoen.2021.106277.

[25] S. Li, N. Yang, N. Liao, Y. Luo, S. Wang, F. Cao, W. Zhou, D. Huang, H. Chen, Doping β-CoMoO₄ nanoplates with phosphorus for efficient hydrogen evolution reaction in alkaline media, ACS Appl. Mater. Interfaces 10 (2018) 37038–37045, https://doi.org/10.1021/acsami.8b13266.

[26] J. Wang, Z. Wei, S. Mao, H. Li, Y. Wang, Highly uniform Ru nanoparticles over N-doped carbon: pH and temperature-universal hydrogen release from water reduction, Energy Environ. Sci. 11 (2018) 800–806, https://doi.org/10.1039/C7EE03345A.

[27] T.L.L. Doan, D.T. Tran, D.C. Nguyen, D.H. Kim, N.H. Kim, J.H. Lee, Rational engineering CoxOy nanosheets via phosphorous and sulfur dual-coupling for enhancing water splitting and Zn-Air battery, Adv. Funct. Mater. 31 (2020) 2007822, https://doi.org/10.1002/adfm.202007822.

[28] C. Lin, J.-L. Li, X. Li, S. Yang, W. Luo, Y. Zhang, S.-H. Kim, D.-H. Kim, S.S. Shinde, Y.-F. Li, Z.-P. Liu, Z. Jiang, J.-H. Lee, In-situ reconstructed Ru atom array on α-MnO₂ with enhanced performance for acidic water oxidation, Nat. Catal. 4 (2021) 1012–1023, https://doi.org/10.1038/s41929-021-00703-0.

[29] Q. Quan, X. Bu, D. Chen, F. Wang, X. Kang, W. Wang, Y. Meng, S. Yip, C. Liu, J. C. Ho, Sequential self-reconstruction of localized Mo species in hierarchical Carbon/Co–Mo oxide heterostructures for boosting alkaline hydrogen evolution kinetics and durability, J. Mater. Chem. A 10 (2022) 3953–3962, https://doi.org/10.1039/D1TA09010K.

[30] T. Ouyang, X.-T. Wang, X.-Q. Mai, A.-N. Chen, Z.-Y. Tang, Z.-Q. Liu, Coupling magnetic single-crystal Co₂Mo₃O₈ with ultrathin nitrogen-rich carbon layer for oxygen evolution reaction, Angew. Chem. Int. Ed. 59 (2020) 11948–11957, https://doi.org/10.1002/anie.202004533.

[31] Q. Liang, L. Zhong, C. Du, Y. Luo, J. Zhao, Y. Zheng, J. Xu, J. Ma, C. Liu, S. Li, Q. Yan, Interfacing epitaxial dinickel phosphide to 2D nickel thiophosphate nanosheets for boosting electrocatalytic water splitting, ACS Nano 13 (2019) 7975–7984, https://doi.org/10.1021/acsnano.9b02510.

[32] C. Wang, H. Lu, Z. Mao, C. Yan, G. Shen, X. Wang, Bimetal schottky heterojunction boosting energy-saving hydrogen production from alkaline water via urea electrocatalysis, Adv. Funct. Mater. 30 (2020) 2000556, https://doi.org/10.1002/adfm.202000556.

[33] L. Li, D. Yu, P. Li, H. Huang, D. Xie, C.-C. Lin, F. Hu, H.-Y. Chen, S. Peng, Interfacial electronic coupling of ultrathin transition-metal hydroxide nanosheets with layered MXenes as a new prototype for platinum-like hydrogen evolution, Energy Environ. Sci. 14 (2021) 6419–6427, https://doi.org/10.1039/d1ee02538d.

[34] C. Lei, Y. Wang, Y. Hou, P. Liu, J. Yang, T. Zhang, X. Zhuang, M. Chen, B. Yang, L. Lei, C. Yuan, M. Qiu, X. Feng, Efficient alkaline hydrogen evolution on atomically dispersed Ni–Nx species anchored porous carbon with embedded ni nanoparticles by accelerating water dissociation kinetics, Energy Environ. Sci. 12 (2019) 149–156, https://doi.org/10.1039/C8EE01841C.

[35] S. Anantharaj, S.R. Ede, K. Karthick, S. Sam Sankar, K. Sangeetha, P.E. Karthik, S. Kundu, Precision and correctness in the evaluation of electrocatalytic water splitting: revisiting activity parameters with a critical assessment, Energy Environ. Sci. 11 (2018) 744–771, https://doi.org/10.1039/C7EE03457A.

[36] Y. Xie, Q. Qian, J. Zhang, J. Li, Y. Li, X. Jin, Y. Zhu, Y. Liu, Z. Li, A. El-Haraiiy, C. Xiao, G. Zhang, Artificial heterointerfaces achieve delicate reaction kinetics towards hydrogen evolution and hydrazine oxidation catalysis, Angew. Chem. Int. Ed. 60 (2020) 5984–5993, https://doi.org/10.1002/anie.202014362.

[37] P. Li, M. Wang, X. Duan, L. Zheng, X. Cheng, Y. Zhang, Y. Kuang, Y. Li, Q. Ma, Z. Feng, W. Liu, X. Sun, Boosting oxygen evolution of single-atomic ruthenium through electronic coupling with cobalt-iron layered double hydroxides, Nat. Commun. 10 (2019) 1711, https://doi.org/10.1038/s41467-019-09666-0.

[38] D. Guo, Z. Wan, Y. Li, B. Xi, C. Wang, TiN@Co₅.₄₇N composite material constructed by atomic layer deposition as reliable electrocatalyst for oxygen evolution reaction, Adv. Funct. Mater. 31 (2020) 2008511, https://doi.org/10.1002/adfm.202008511.

[39] V.H. Hoa, D.T. Tran, D.C. Nguyen, D.H. Kim, N.H. Kim, J.H. Lee, Molybdenum and phosphorous dual doping in cobalt monolayer interfacial assembled cobalt nanowires for efficient overall water splitting, Adv. Funct. Mater. 30 (2020) 2002533, https://doi.org/10.1002/adfm.202002533.

[40] M. Wang, C.-L. Dong, Y.-C. Huang, S. Shen, Operando spectral and electrochemical investigation into the heterophase stimulated active species transformation in transition-metal sulfides for efficient electrocatalytic oxygen evolution, ACS Catal. 10 (2020) 1855–1864, https://doi.org/10.1021/acscatal.9b05170.

[41] L. Wu, L. Yu, F. Zhang, B. McElhenny, D. Luo, A. Karim, S. Chen, Z. Ren, Heterogeneous bimetallic phosphide Ni₂P-Fe₂P as an efficient bifunctional catalyst for water/seawater splitting, Adv. Funct. Mater. 31 (2021) 2006484, https://doi.org/10.1002/adfm.202006484.

stable CoMoP@C electrocatalyst superior to Pt/C, Energy Environ. Sci. 10 (2017) 788–798, https://doi.org/10.1039/C6EE03768B.

[42] L. An, J. Feng, Y. Zhang, R. Wang, H. Liu, G.-C. Wang, F. Cheng, P. Xi, Epitaxial heterogeneous interfaces on N-NiMoO$_4$/NiS$_2$ nanowires/nanosheets to boost hydrogen and oxygen production for overall water splitting, Adv. Funct. Mater. 29 (2019) 1805298, https://doi.org/10.1002/adfm.201805298.

[43] X. Ji, Y. Lin, J. Zeng, Z. Ren, Z. Lin, Y. Mu, Y. Qiu, J. Yu, Graphene/MoS$_2$/FeCoNi (OH)$_x$ and graphene/MoS$_2$/FeCoNiP$_x$ multilayer-stacked vertical nanosheets on carbon fibers for highly efficient overall water splitting, Nat. Commun. 12 (2021) 1380, https://doi.org/10.1038/s41467-021-21742-y.

[44] L. Deng, K. Zhang, D. Shi, S. Liu, D. Xu, Y. Shao, J. Shen, Y. Wu, X. Hao, Rational design of schottky heterojunction with modulating surface electron density for high-performance overall water splitting, Appl. Catal., B 299 (2021), 120660, https://doi.org/10.1016/j.apcatb.2021.120660.

[45] J. Xu, Z. Ju, W. Zhang, Y. Pan, J. Zhu, J. Mao, X. Zheng, H. Fu, M. Yuan, H. Chen, R. Li, Efficient infrared-light-driven CO$_2$ reduction over ultrathin metallic Ni-doped CoS$_2$ nanosheets, Angew. Chem. Int. Ed. 60 (2021) 8705–8709, https://doi.org/10.1002/anie.202017041.

[46] G. Zhang, B. Wang, L. Li, S. Yang, Phosphorus and yttrium codoped Co(OH)F nanoarray as highly efficient and bifunctional electrocatalysts for overall water splitting, Small 15 (2019), e1904105, https://doi.org/10.1002/smll.201904105.
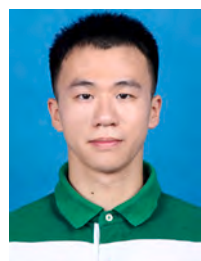
**Xiuming Bu** is currently a postdoctoral fellow at City University of Hong Kong. He received his phd degree and master degree in materials science and engineering from the City University of Hong Kong and University of Shanghai for Science and Technology in 2020 and 2017, respectively. His research intersets include the fabrication of nanomaterials and their applications in electronics and energy conversion.



**Quan Quan** is currently a Ph.D. student in the Department of Materials Science and Engineering at the City University of Hong Kong. Her research interests mainly focus on the synthesis of nano-structural catalysts for applications in electrocatalysis and related interdisciplinary sustainable chemistry.



**Wei Wang** is currently a Ph.D. student in the Department of Materials Science and Engineering at City University of Hong Kong. He received his BS degree in Electronic Science and Technology from Anhui Jianzhu University in 2012 and an MS degree in Materials Engineering from Tongji University in 2015. His research mainly involves the fabrication of nanomaterials, including III-V semiconductor nanowires and 2D materials, along with nanomaterial-based devices regarding the integration of field-effect transistor and near-infrared photoconductors/photodiodes, etc.



**Yuxuan Zhang** is currently a Ph.D. student in the Department of Materials Science and Engineering at the City University of Hong Kong. He received his BS and MS degree from Chongqing University in 2017 and 2020, respectively. His research interests mainly focus on the computational study of materials and synthesis of 2D materials with their novel devices for transistors, photodetectors, etc.



**Johnny C. Ho** is a professor of Materials Science and Engineering at the City University of Hong Kong. He received his B. S. degree in chemical engineering and his M.S. and Ph.D. degrees in materials science and engineering from the University of California, Berkeley, in 2002, 2005, and 2009, respectively. From 2009–2010, he was a postdoctoral research fellow in the Nanoscale Synthesis and Characterization Group at Lawrence Livermore National Laboratory. His research interests focus on synthesis, characterization, integration, and device applications of nanoscale materials for various technological applications, including nanoelectronics, sensors, and energy harvesting.



**Fei Wang** is currently working as a postdoctoral researcher in the Department of Materials Science and Engineering at the City University of Hong Kong. His research interests mainly focus on the design and growth of 2D materials, along with nanomaterials-based devices regarding the infrared photoconductors/photodiodes.